JOURNAL OF MATERIALS SCIENCE 32 (1997) 4979–4984

Preparation, electrochemical, photoelectrochemical and solid-state characteristics of indium-incorporated TiO_2 thin films for solar cell fabrication

W. A. BADAWY
Department of Chemistry, Faculty of Science, University of Kuwait, P.O. Box 5969 Safat, 13060 Kuwait

Titanium dioxide thin films were prepared by the spray-pyrolysis technique, which permitted the convenient incorporation of foreign materials into the oxide matrix during its formation. Pure and indium-incorporated films of different thickness were prepared. The presence of indium in the TiO_2 film affected the characteristics of that material. The effect of incorporation was reflected in the improvement of the properties of the n-Si/oxide heterojunction. The prepared n-Si/TiO_2-In solar cells exhibited better fill factor and solar conversion efficiency than those with pure TiO_2. The electrochemical properties of the prepared oxide films revealed that the charge transfer step at the oxide/electrolyte interface leads to the deterioration in quality of the photoanode. The improved characteristics of the heterojunction n-SiO_2/oxide in the presence of indium incorporation offset the limitation of the photoelectrochemical cell due to the slow charge transfer step at the TiO_2/electrolyte junction.

1. Introduction

Titanium oxide is one of the most familiar and attractive materials in solar cell fabrication. The excellent properties of TiO_2 as an anti-reflector and very stable material against corrosion damage make its utilization in the fabrication of solar cells for terrestrial and extra-terrestrial applications an important subject worthy of intensive studies. Efficient, stable and low-cost solar cells represent the aim of many investigations [1]. The stability of TiO_2 against chemical attack and corrosion extends its applications to photoelectrolytic cells [2–6]. Incorporation of foreign atoms into the oxide film is known to induce substantial modifications in its semiconductor properties. This phenomenon has been sporadically investigated in connection with semiconductor electrodes for photoelectrolysis devices [7–14]. The incorporation was essentially aimed at extending the response of some wide band-gap valve metal oxide layers like TiO_2 or Nb_2O_5 to the visible region of the spectrum. Doping of TiO_2 with tungsten was found to shift the absorption of the material towards the ultraviolet region [15]. Addition of chromium or cadium extends the photoactive range of the oxide into the visible part of the spectrum [2, 4, 16, 17]. In one of our publications [14], the effect of indium incorporation into the TiO_2 matrix on the solid-state characteristics of the material was investigated. In this work, pure and indium-incorporated TiO_2 thin films were used as a heterojunction with n-Si. The photovoltaic and photoelectrochemical properties of the prepared heterojunctions were studied. The effect of indium-incorporation on the characteristics of the prepared devices has been discussed.

2. Experimental procedure

Pure and indium-incorporated thin films were prepared on different substances conveniently and reproducibly by using the spray/chemical vapour deposition (CVD) technique described elsewhere [18, 19]. The pyrolysis reaction

$$TiCl_{4(g)} + 2H_2O_{(g)} \xrightarrow{723\,K} TiO_{2(s)} + 4HCl_{(g)} \quad (1)$$

produces glass-like, transparently clear films with an interference colour depending on the thickness of the prepared film. The spray solution consisted of 0.5 mol l^{-1} $TiCl_4$ dissolved in ethanol (96%). Indium incorporation was achieved by the addition of $InCl_3$ which made the solution 0.03, 0.06, 0.09 and 0.12 mol l^{-1} with respect to indium chloride. The flow rate of the deriving gas (nitrogen) was 5 l min^{-1} and the substances either glass, fused silica, glassy carbon (GC) or silicon were kept at 723 K throughout the spraying process.

For optical measurements, the glass specimens (2.2 cm × 1.2 cm × 0.2 cm) were employed. The measurements were carried out using a double-beam spectrophotometer (Perkin–Elmer Lambda 4B

UV/VIS) over the 200–900 nm wavelength range. To minimize reflection, a very thin film was taken as the reference sample, while a thicker one was the test sample [20]. For each concentration of indium in the TiO_2 films, the band-gap energy, E_g, refractive index, n, extinction coefficient, K, and thickness, δ, were estimated from the measured transmittance data. The conductivity measurements were carried out using an electrometer (Cary 401, vibrating reed electrometer). The contacts were made by evaporating two rectangular gold contacts (0.15 cm × 0.3 cm) on to the TiO_2 film front [13].

For photovoltaic investigations, the films were deposited on polished silicon wafers (Wacker-Burghausen, Germany) typically 0.2 cm^2, of orientation $\langle 1\,0\,0 \rangle$, resistivity of 0.6–1.4 Ωcm. They were pretreated with a standard solution of formic acid/H_2O and hydrofluoric acid [21]. The evaporated gold was used as the forward contacts of the photovoltaic cell and the back contacts were made by using In–Ga alloy followed by silver paste. The investigation of the electrochemical behaviour of the oxide films was carried out by depositing the TiO_2 or TiO_2–In on to glassy carbon discs (Sigri, Meitingen, Germany, diameter 0.8 cm, thickness 0.3 cm; polished with diamond paste down to 1 μm; washed in alcohol and acetone in an ultrasonic bath). The discs were mounted in stainless steel holders of a rotating disc electrode system and insulated with teflon tape so that the oxide-coated circular area was exposed to the solution. In order to minimize structure fluctuations, the same experimental parameters for the preparation of TiO_2 or TiO_2–In films on glass, silicon or GC were always chosen. A conventional potentiostatic set-up was used to trace the current density–potential behaviour of the cells. Illumination was carried out using a 150 W xenon lamp coupled with an Oriel solar simulator and filter, to simulate the solar spectrum. The photovoltaic current density–potential characteristics were corrected for R_s (the series resistance) as described previously [18]. Other experimental parameters were as reported elsewhere [18, 19].

3. Results

3.1. Resistivity measurements

The resistivity of the prepared films was found to decrease as the film thickness increases. Fig. 1 presents the variation of the resistance of pure and indium-incorporated TiO_2 with the thickness of the film. Specific conductance calculations showed that the homogeneity of the prepared film depends on its thickness. For relatively thick TiO_2 films ($\delta \geqslant 100$ nm), a value of $1 \times 10^{-3}\,\Omega^{-1}\,cm^{-1}$ for the specific conductance of films prepared from ethyl acetate solutions was obtained [19]. Films prepared from alcoholic solutions are relatively less conducting. TiO_2 doped with indium is more conducting (cf. Fig. 1). The presence of indium in the TiO_2 matrix increases the specific conductivity of the films by about three orders of magnitudes, even for very thin oxide films ($\delta \leqslant 50$ nm).

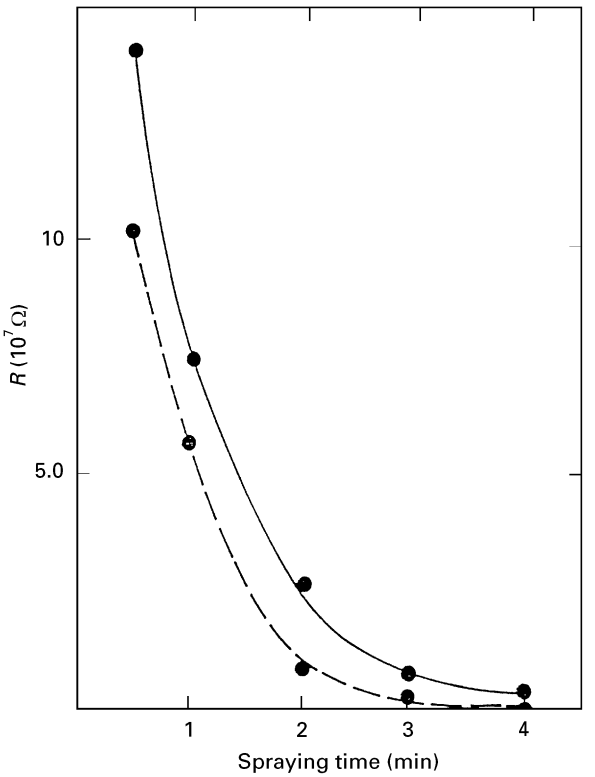

Figure 1 Effect of film thickness on the resistance of (—) pure TiO_2 and (– – –) TiO_2–In.

3.2. Optical characteristics of the films

3.2.1. Transmittance measurements

The structure of the prepared film depends on its thickness. The presence of interference extrema in the transmittance, % T, versus wavelength, λ, curves indicates the presence of crystalline structure. Films which do not show extrema are amorphous [22]. Fig. 2 presents the % T as a function of λ for pure TiO_2 of different thickness (Fig. 2a) and for TiO_2–In (Fig. 2b and c). Irrespective of the concentration of indium, all films of $\delta \leqslant 70$ nm are amorphous, i.e. no interference extrema could be observed. For thicker films ($\delta > 70$ nm), interference extrema were recorded and found to depend on both the thickness of the film and the concentration of indium therein. Thus the crystallinity of the film increases as the concentration of indium increases (compare Fig. 2b and c) and also as the thickness of the film increases. Comparison of the curves of Fig. 2 shows that at $\lambda \approx 500$ nm, the transmittance of the film increases up to 96% in the presence of indium (0.09 $mol\,l^{-1}$). Further increase in the indium concentration ($> 0.12\,mol\,l^{-1}$) led to the deterioration of the optical properties of the film. The increased amount of incorporated foreign atoms in the oxide matrix may lead to increased absorption of light and hence to a decrease in the transmittance of the samples [23]. The effect of the thickness on the transmittance of the film is clearly reflected in the curves presented in Fig. 2a, b or c. Considering Fig. 2a, the %T of films of $\delta \approx 70$ nm is in the range of 70% at a wavelength of 550 nm. Doubling the film thickness, i.e. for $\delta \approx 140$ nm, the transmittance increases to about 90%. This is due to the increased crystallinity of the film with the increase of the film thickness. The

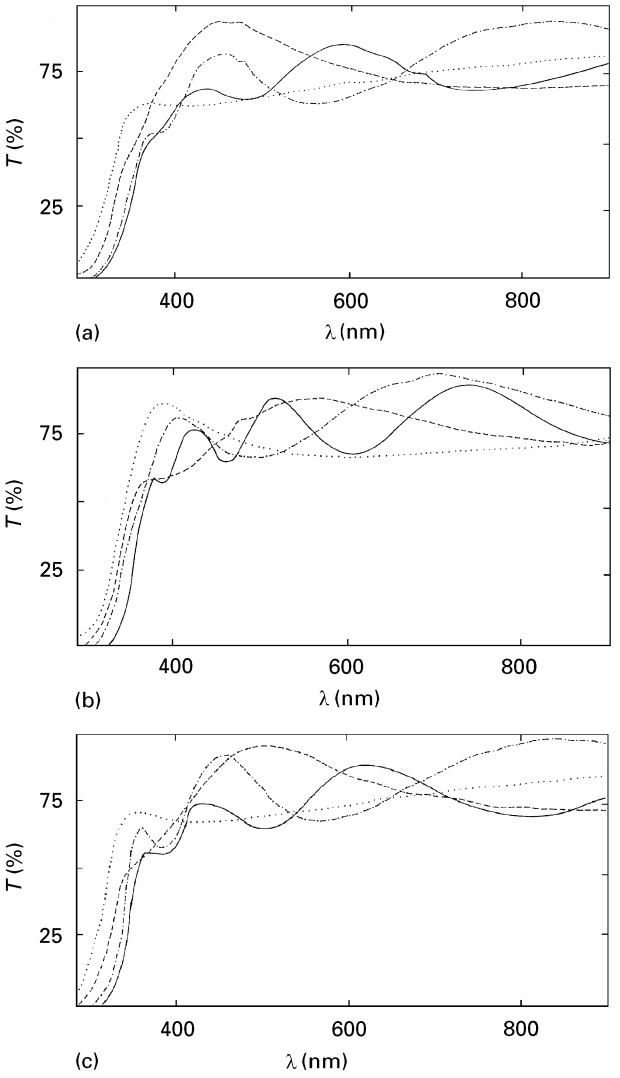

Figure 2 Transmittance (% T) of the prepared films with different thicknesses: (....) 70 nm, (- - -) 110 nm, (- · - · -) 140 nm, (—) 170 nm. (a) Pure, TiO_2, (b) TiO_2–In (0.03 mol $InCl_3$/litre solution), (c) TiO_2–In (0.09 mol $InCl_3$/litre solution).

presence of amorphous characteristics is accompanied by a decrease in the transmittance. Exceeding a certain thickness ($\delta \geqslant 170$ nm), the absorbance of the film increases again and hence the transmittance decreases [13].

3.2.2. Refractive index, n, extinction coefficient, K and thickness, δ

The optical parameters n and K, as well as the thickness, δ, of the prepared films can be obtained from the % T versus λ data. As can be seen in Fig. 2, the % T versus λ curves possess an envelope shape, passing interference extrema. From this envelope n, K and δ for TiO_2 films can be calculated [24]. Considering any envelope, $T^+(\lambda)$ and $T^-(\lambda)$ couples can be used to calculate $n(\lambda)$ and $K(\lambda)$. The thickness, δ, can be obtained from the values of T^+ and T^- corresponding to the interference extrema in the very weak absorption region [20, 22, 24]. Applying the calculations reported before [13] to the results presented in Fig. 2, the refractive index, n, and extinction coefficient, K, of the prepared TiO_2 films at different thicknesses, either pure (Fig. 2a) or containing different concentrations of indium (Fig. 2b and c), can be calculated. At a constant film thickness, the refractive index decreases as the wavelength increases. The relation consists of two parts. The first corresponds to long wavelength ($\lambda \geqslant 550$ nm) and shows a non-dispersive, approximately steady part of a nearly constant value of n. The value of the refractive index decreases as the extent of indium incorporation increases. The calculated steady values for $\lambda \geqslant 550$ nm range between 2.25 for pure TiO_2 layers and 2.10 for TiO_2 containing approximately 1% In. In the second part, i.e. at shorter wavelength ($\lambda < 500$ nm) fluctuations, especially near the ultraviolet region were observed and higher values for n were estimated. This behaviour is similar to the behaviour of fluorine-incorporated SnO_2 films [25]. The calculated values for the extinction coefficient, K, of the same film ($\delta \approx 100$ nm) show that K decreases as the amount of indium in the TiO_2 matrix increases. The relation between K and λ for the different films did not show any fluctuations, and parallel curves for the different concentrations of indium were obtained. The calculated values for K for the different films range between 0.515 for pure TiO_2 and 0.380 for the 1% indium-incorporated TiO_2. The calculated values of the refractive index, n, and extinction coefficient, K, for indium-incorporated TiO_2 thin films ($\delta \approx 100$ nm) at $\lambda = 550$ nm are presented in Table I.

3.2.3. Energy-gap calculations

The energy gap of the prepared films was calculated using the transmittance ratio data according to

$$T_{1-2} = e^{-\alpha\Delta\delta} \quad (2)$$

where T_{1-2} is the transmittance ratio, Δδ is the thickness difference between δ_2 and δ_1, and α is the absorption coefficient. αΔδ can be determined accurately without determining Δδ [26]. The energy gap was obtained by extrapolating the $(\alpha\Delta\delta)^2$ versus photon energy, $h\nu$, plots. For direct allowed transition, the variation of the absorption coefficient with photon energy is given by

$$\alpha = \alpha_0(h\nu - E_g)^{1/2} \quad (3)$$

where $h\nu$ and E_g are the photon and gap energies, respectively. α_0 is a constant independent of the photon energy [13, 27]. Photons of energy $h\nu \geqslant E_g$ can be absorbed by the oxide film. Fig. 3 represents the relation between $(\alpha\Delta\delta)^2$ and $h\nu$ at different film thickness of pure TiO_2 (Fig. 3a) and TiO_2–In (Fig. 3b). The value of the band-gap energy was obtained by extrapolating the straightest portion of the line to

TABLE I Values of the refractive index, n, and the extinction coefficient, K, for TiO_2–In thin films ($\delta \approx 100$ nm) at $\lambda = 500$ nm

In conc. ($mol l^{-1}$)	n	K
0.03	2.222	0.515
0.06	2.175	0.475
0.09	2.152	0.420
0.12	2.104	0.380

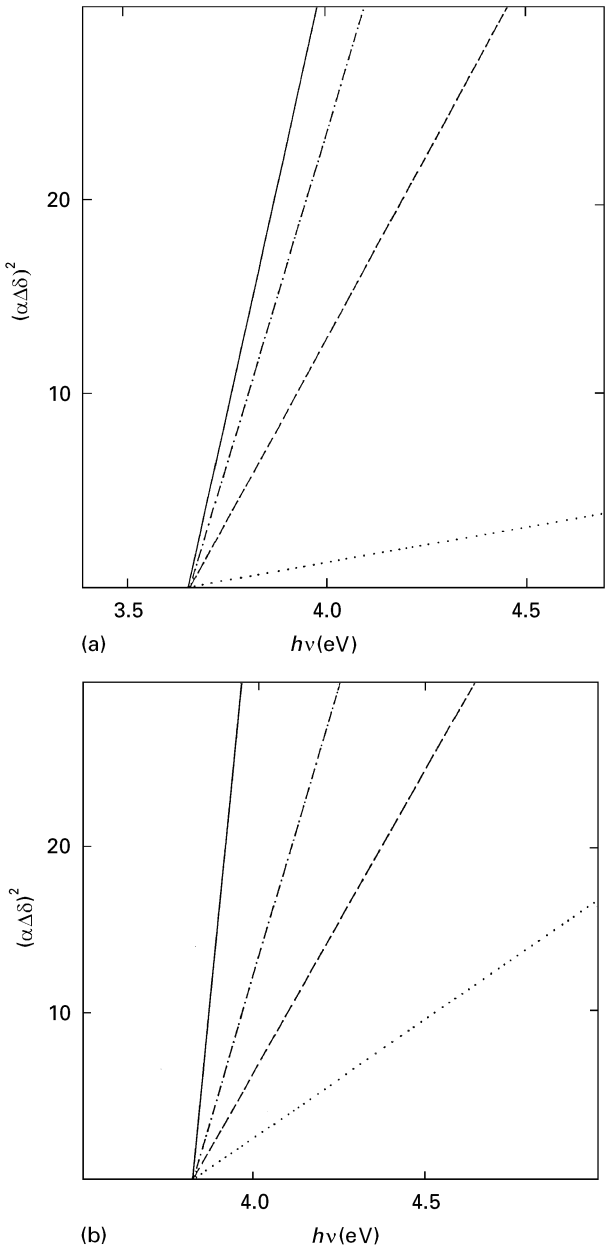

Figure 3 Variation of the square of the absorption coefficient of the prepared oxide films with different thicknesses: (....) 70 nm, (– – –) 110 nm, (- · -· -) 110 nm, (—) 170 nm. (a) Pure TiO_2, (b) TiO_2–In (0.12 mol $InCl_3$/litre solution).

$(\alpha\Delta\delta)^2 = 0$. As can be seen, the energy gap is independent of the film thickness [13]. Indium incorporation led to an increase in the band gap energy of about 5%. The effect of the amount of indium on the band-gap energy of TiO_2 is presented in Fig. 4. The increase of the extrapolated value of the band-gap energy may be attributed to structural changes in the polycrystalline TiO_2 layers. The relatively large band-gap energy of pure TiO_2 ($\sim$3.64 eV) is due to the polycrystalline nature of the prepared films [28].

3.3. Photovoltaic characteristics of the prepared cells

Pure and indium-incorporated TiO_2 films ($\delta \approx 100$ nm) were deposited on to n-Si as described in Section 2. Typical power characteristics of both n-Si/TiO_2 and n-Si/TiO_2–In solar cells under

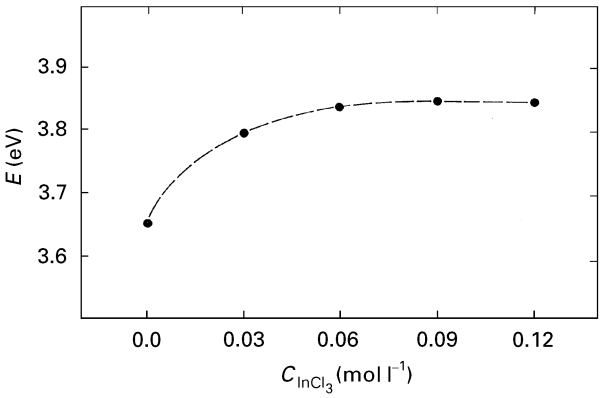

Figure 4 Effect of the concentration of $InCl_3$ in the spraying solution on the band-gap energy of the prepared TiO_2 thin films ($\delta \sim 100$ nm)

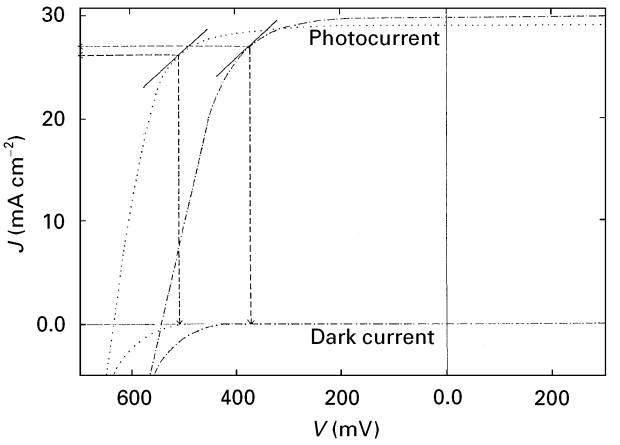

Figure 5 Typical power characteristics of (- · - · -) n-Si/TiO_2 and (···) n-Si/TiO_2–In photovoltaic cells. Illumination intensity 100 mW cm^{-2} (AM1).

a 100 mW cm^{-2} simulated solar spectrum (AM1) are presented in Fig. 5. The presence of indium in the TiO_2 matrix had a significant effect on the power characteristics of the prepared cells. In spite of the fact that the extent of indium incorporation did not exceed 1% as determined by ESCA [29], the power characteristics of the cells are significantly improved. The fill factor (FF) was increased from $\sim$0.6 (pure TiO_2) to 0.82 (TiO_2-In). The solar conversion efficiency reached 14.1% for the indium-containing solar cells, i.e. an increase of about 40% could be achieved with indium incorporation. The increased solar efficiency is solely due to the improved open-circuit potential of the cell: an increase over 100 mV was measured. The photocurrent was not significantly affected by indium incorporation. A typical value of 28 mA cm^{-2} was obtained. The same effect was observed on using antimony as dopant for the TiO_2 barrier layers [14].

3.4. Electrochemical behaviour of the prepared oxide films

For the electrochemical investigations, the oxide films were deposited on to GC substrates and mounted as electrodes in the holders of the rotating disc system. Fig. 6 presents the current density–potential behaviour of the pure and indium-incorporated TiO_2 films

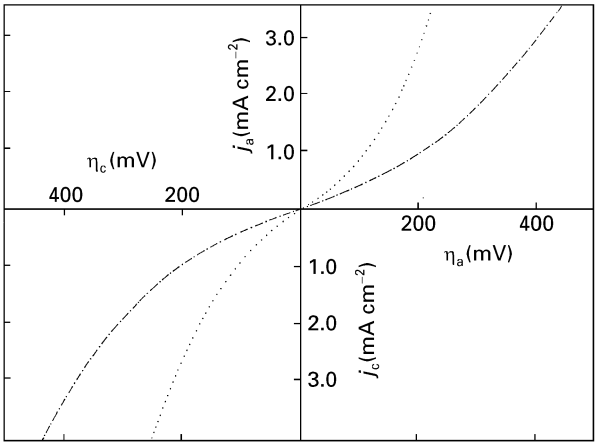

Figure 6 Current density–potential curves of (– · –) pure TiO_2 and (···) TiO_2–In thin films ($\delta \approx 100$ nm) in 0.05 M $K_3Fe(CN)_6$/0.05 M $K_4Fe(CN)_6$/0.5 M KNO_3. Scan rate 50 mV s^{-1}, rotation speed 2500 r.p.m. at 298 K.

in a simple one-electron electrolyte system consisting of 0.05 M $K_3Fe(CN)_6$/0.05 M $K_4Fe(CN)_6$/0.5 M KNO_3. Analysis of the results of Fig. 6 shows that the overpotential near the equilibrium potential obeys the linear approximation of the Butler–Volmer equation [30] and the charge transfer resistance, R_{CT}, can be calculated according to Equation 4

$$R_{CT} = \eta_{CT}/j = (RT/F)(1/nj_0) \quad (4)$$

where η_{CT} is the charge transfer overpotential, j is the current density, j_0 is the exchange current density, n is the number of electrons involved in the electrode process, F, R, and T have their usual meanings. The results reveal that the presence of indium in the oxide film decreases the charge transfer resistance and hence the rate of the charge transfer at the electrode/electrolyte interface increases by $\sim 40\%$ (cf. Fig. 7a). At overpotentials more than 100 mV, i.e. $|\eta| > 100$ mV, Tafel behaviour was observed. Analysis of the results according to the Tafel approximation (Equation 5) is presented in Fig. 7b

$$j = j_0 \exp[(\alpha nF/RT)\eta_{CT}] \quad (5)$$

The plots of Fig. 6b have slopes ranging between 400 mV/decade (pure TiO_2 films) and 160 mV/decade (TiO_2–In films). The high values of the Tafel slopes are due to change transfer limitations across the electrode (n-type semiconductor)/electrolyte interface [14, 31].

3.5. The photoelectrochemical behaviour of the prepared cells

The improved electrochemical characteristics of the indium-incorporated TiO_2 films are reflected in the photoelectrochemical behaviour of these samples as photoanodes. The photocurrent–potential characteristics of n-Si/TiO_2/electrolyte and n-Si/TiO_2–In/electrolyte photoanodes are presented in Fig. 8. As was observed in the photovoltaic cells (Section 3.3), the foreign-atom incorporation in the TiO_2 had negligible effect on the saturation current and the measured

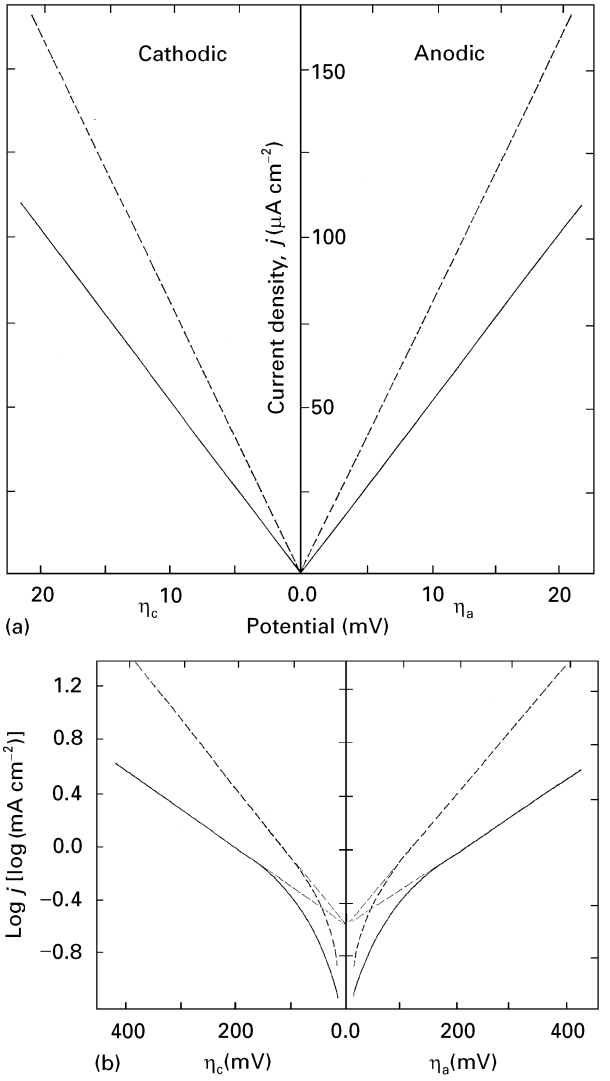

Figure 7 (a) Current density–potential behaviour of (—) pure TiO_2 and (- - -) TiO_2–In rotating discs near the equilibrium potential in the $Fe(CN)_6^{3-/4-}$ redox system at 298 K. (b) Tafel plots of (—) pure TiO_2 and (- - -) TiO_2–In rotating discs in the $Fe(CN)_6^{3-/4-}$ redox system at 298 K.

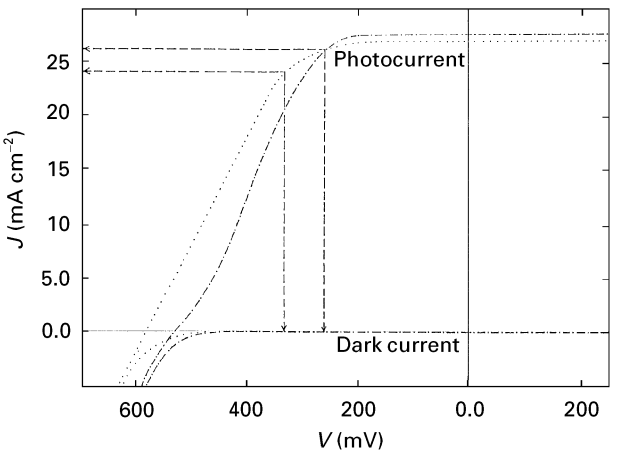

Figure 8 Typical power characteristics of the (—) n-Si/TiO_2 and (- - -) n-Si/TiO_2–In photoanodes in the $Fe(CN)_6^{3-/4-}$ redox electrolyte at 298 K. Scan rate 50 mV s^{-1}, rotation speed 2500 r.p.m. and illumination 100 m W cm^{-2} (AM1).

value for all tested samples (either pure TiO_2 or TiO_2–In) lies between 27 and 28 mA cm^{-2} under AM1 illumination. The decrease in the charge transfer resistance at the electrode/electrolyte interface in the

presence of indium incorporation has led to an improvement of the fill factor of the photoelectrochemical cells. The fill factor was increased from 0.46 (pure TiO_2) to 0.58 (TiO_2–In) i.e. about 26% increase. A better fill factor of a solar cell will lead to a better solar conversion efficiency. The photoelectrochemical conversion efficiency of the prepared cells was increased from 6.8% (pure TiO_2) to 8.6% (TiO_2–In).

4. Discussion

The presence of foreign atoms in the TiO_2 matrix improves its characteristics in a way that a relevant practical application of this material in solar energy converters could be achieved. The conductivity of the material increases. The rate of the reactionless one-electron transfer depends on a quantum mechanical frequency factor related to the tunnel probability of the electron and the density of electronic states in the oxide layer energetically suitable for the redox system. Increasing the concentration of charge carriers in the semiconducting TiO_2 film is likely to increase the tunnel probability by decreasing the thickness of the space-charge layer of the semiconductor. This corresponds to an increase of the electrochemical rate constant of the redox reaction occurring at the electrode/electrolyte interface. The electrochemical charge transfer process then leads to a deterioration of the cell quality. The slopes of the Tafel plots, which are related to the charge transfer coefficient, α, and normally used to characterize charge transfer processes involving absorption/chemisorption intermediates [32, 33], are given by

$$b = 0.059/\alpha n \quad (6)$$

at 298 K, where b is the Tafel slope.

The values of b and α are improved due to the incorporation of indium in the oxide film matrix. The increase in the rate of charge transfer at the oxide/electrolyte interface has led to a better fill factor and improved solar conversion efficiency of the photoelectrochemical cells containing indium. The analysis of the electrochemical and photoelectrochemical results demonstrate the usefulness of the concept used [26]. This concept is based on considering heterojunctions like n-Si/TiO_2 as a combination of photovoltaic and electrochemical characteristics, which can be treated separately. The presence of indium in the TiO_2 films was shown to improve the photovoltaic characteristics and also to increase the rate of the charge transfer step in the electrochemical system. The improved fill factor and the increase in the solar conversion efficiency of the prepared cells make TiO_2–In thin films important components in the solar cell fabrication.

5. Conclusion

Incorporation of TiO_2 with indium leads to an increase in the conductivity of the oxide. The rate of the charge transfer step at the oxide/electrolyte interface increases and hence the catalytic properties of the oxide improves. The improved oxide characteristics have led to improved photovoltaic and photoelectrochemical systems for practical use.

Acknowledgement

Financial support from the Alexander von Humboldt-Stiftung is gratefully acknowledged.

References

1. J. H. WOHLGEMUTH, D. B. WARFIELD and G. A. JOHNSON, *IEEE* (1982) 809.
2. A. MONNIER and J. AUGUSTINSKI, *J. Electrochem. Soc.* **127** (1980) 1576.
3. A. FUJISHIMA and K. HONDA, *Nature* **238** (1972) 37.
4. A. K. GHOSH and H. P. MARUSKA, *J. Electrochem. Soc.* **124** (1977) 1516.
5. H. P. MARUSKA and A. K. GHOSH, *Solar Energy Mater.* **1** (1979) 237.
6. Y. MATSUMOTO, J. KURIMOTO, Y. AMAGASAKI and E. SATS, *J. Electrochem. Soc.* **127** (1980) 2360.
7. L. HARRIS and R. WILSON, *Am. Rev. Mater. Sci.* **8** (1978) 99.
8. M. P. MARUSKA and A. K. GHOSH, *Solar Energy* **20** (1979) 433.
9. J. G. MARROIDES, *Mater. Res. Bull.* **13** (1978) 1379.
10. K. RAJESHWAR, P. SINGH and J. DU BOW, *Electrochim. Acta* **23** (1978) 1117.
11. A. J. NOZIK, *Ann. Rev. Phys. Chem.* **29** (1978) 189.
12. M. TOMKIEWICZ and H. FAY, *Appl. Phys* **18** (1979) 1.
13. W. A. BADAWY, R. S. MOMTAZ and E. M. EL-GIAR, *Phys. Status Solidi* (*a*) **118** (1990) 197.
14. W. A. BADAWY, *Solar Energy Mater. Solar Cells* **28** (1993) 293.
15. M. S. WRIGHTON, D. S. GINLEY, P. T. WOLCZANSKI, A. B. ELLIS, D. L. MORSE and A. LINZ, *Proc. Nat. Acad. Sci. USA* **72** (1975) 1518.
16. A. K. GHOSH and M. P. MARUSKA, in "Solar Energy" edited by J. B. Berkowitz and I. A. Lesk (Electrochemical Society Softbound Proceedings Series, Princeton, NJ, 1976) p. 92.
17. C. STADLER, A. MONNIER and J. AUGUSTYNSKI, in "Extended Abstracts of the 2nd International Conference on the Photochemical Conversion and Storage of Solar Energy", Cambridge, UK, 10–12 August 1978, p. 81.
18. W. A. BADAWY, F. DECKER and K. DOBLHOFER, *Solar Energy Mater.* **8** (1983) 363.
19. W.A. BADAWY and E.A. EL-TAHER, *Thin Solid Films* **158** (1988) 277.
20. O. P. AGNIHOTRI, M. T. MOHAMMED, A. K. ABBAS and K. I. ARSHAK, *Solid State Commun* **47** (1983) 195.
21. D. PULFREY, *IEEE Trans. Electron. Dev.* **ED-25** (1978) 1308.
22. H. DEMIRYONT and K. E. NIETRING, *Solar Energy Mater.* **19** (1989) 79.
23. W. A. BADAWY, H. H. AFIFY and E. M. EL-GIAR, *J. Electrochem. Soc.* **137** (1990) 1592.
24. H. DEMIRYENT, J. R. SITES and K. GEIB, *Appl. Optics* **24** (1985) 490.
25. H. H. AFIFY, R. S. MOMTAZ, W. A. BADAWY and S. N. NASSER, *J. Mater. Sci. Materials in Electronics* **2** (1991) 40.
26. A. K. ABBAS and M. T. MOHAMMED, *J. Appl. Phys.* **59** (1986) 1641.
27. J. BARDEEN, F. J. SLATT and C. J. HALL, in "Photoconductivity Conference" (Wiley, New York, 1956) p. 146.
28. W. A. BADAWY, *Ind. J. Technol.* **29** (1991) 235.
29. F. DECKER, M. FRACASTORO-DECKER, W. BADAWY, K. DOBLHOFER and H. GERISCHER, *J. Electrochem. Soc.* **130** (1983) 2173.
30. A. J. BARD and L. R. FAULKNER, "Electrochemical Methods-Fundamentals and Applications" (Wiley, New York, 1980) Ch. 3.
31. W. A. BADAWY, *Ind. J. Technol.* **24** (1986) 118.
32. K. UOSAKI and M. KIAI, *J. Electrochem. Soc.* **130** (1983) 985.
33. H. GERISCHER, *J. Electrochem. Soc.* **130** (1983).

Received 31 October 1995
and accepted 24 April 1996